Astron. Astrophys. 349, 956–960 (1999)

ASTRONOMY AND ASTROPHYSICS

Coronal hole diagnostics out to $8R_\odot$

J.G. Doyle, L. Teriaca, and D. Banerjee

Armagh Observatory, College Hill, Armagh BT61 9DG, Ireland (jgd, lte, dipu@star.arm.ac.uk)

Received 27 November 1998 / Accepted 27 May 1999

Abstract. The Si VIII line width measurements and N_e estimates based on SUMER observations are combined with LASCO and UVCS output to provide an overview of its variations with height above a polar coronal hole. From the combined dataset we find a radial dependence of the electron density, in the range 1–2 $R_\odot$ as r^{-8}, from 2 to 4 $R_\odot$ as r^{-4} and then as r^{-2}. Combining the Si VIII half width at 1/e of the peak intensity with the UVCS O VI half width, we find a small increase of the half width from 1 to 1.2 $R_\odot$, then a plateau until 1.5 $R_\odot$, thereafter a sharp increase until 2 $R_\odot$, finally a more gradual increase reaching 550 km s^{-1} at 3.5 $R_\odot$. Our data suggests that the MHD waves responsible for the excess line broadening tends to become non-linear as it reaches 1.2 $R_\odot$.

Key words: waves – Sun: corona – Sun: UV radiation

1. Introduction

The measurement of line widths can provide information concerning ion temperatures, sub-resolution turbulent motions and velocity fluctuations associated with magnetohydrodynamic (MHD) waves in the corona. Line width variations combined with simultaneous electron density estimates, provides a very powerful diagnostic for the solar corona. In two previous papers we have reported such observations off the Western limb (Doyle et al. 1998; hereafter DBP) and above a Coronal Hole (Banerjee et al. 1998; hereafter BTDW) based on Si VIII lines observed with SUMER (Wilhelm et al. 1995) onboard *SOHO*. Doschek et al. (1997) have derived electron densities as a function of height in the north and south polar coronal holes. They find that for distances of a few arc seconds outside the solar limb, the average line of sight electron densities in the coronal holes are about a factor of 2 lower than in quiet sun regions. Electron densities similar to those derived from the Si VIII lines are reported by Fludra et al. (1999a,b) and Doyle et al. (1999) based on Si IX data obtained with the CDS instrument onboard *SOHO* (Harrison et al. 1995). Wilhelm et al. (1998) have deduced electron temperatures, densities and ion velocities in plumes and interplume regions of coronal holes. Recently Warren & Hassler (1999) have used Si III, Mg VIII, Si VIII and Mg IX line ratios for electron density measurements. In an earlier study, Hassler et al. (1990) presented line profiles of coronal lines from Mg X 609/625 Å up to $\sim$ 140,000 km above the limb.

In the coronal hole (see BTDW), the line width data show that the non-thermal line-of-sight velocity increases from 27 km s^{-1} at 27 arc sec., above the limb to 46 km s^{-1} some 250 arc sec (*i.e.* $\sim$180,000 km) above the limb. The electron density shows a decrease from 1.1 10^8 cm^{-3} to 1.6 10^7 cm^{-3} over the same distance. It was shown by DBP and BTDW that the Si VIII non-thermal velocity was inversely proportional to the quadratic root of the electron density, in excellent agreement with that predicted for undamped radially propagating Alfvén waves. The Western limb data showed a similar trend. Several questions arise from this work, e.g. how representative are the Si VIII lines of coronal hole conditions near the limb? How do these observations of line width and electron density out to 1.25 $R_\odot$ compare with measurements further off-limb? We address these issues by looking at additional SUMER data out to 1.38 $R_\odot$ coupled with measurements obtained from LASCO and UVCS. This allows us to investigate physical conditions of the solar corona and the coronal-heliospheric interface. Earlier observations of Skylab and more recently *SOHO*/UVCS observations (Cranmer et al. 1999) have established that the fast solar wind originates from coronal holes, while the slow wind is associated with bright equatorial streamers and a number of dramatic transient events such as coronal mass ejections (CMEs). We concentrate here on the coronal hole region in the solar minimum phase (during Nov-Dec '96). All solar wind modelling requires knowledge of both the electron density and non-thermal velocity at the base of the coronal hole as boundary conditions. We hope that our results will provide input parametric values for such solar wind modelling.

2. Observations and data reduction

SUMER is a normal incidence spectrograph operating over the wavelength range 450 Å to 1610 Å, details can be obtained from Wilhelm et al. (1995). The dates of the observations discussed here, their locations, pointing, slit sizes and exposure times are given in BTDW.

Briefly, the data was acquired above a north polar coronal hole (NPCH) on 4 November 1996 and 10 December 1996. Sequences in the NPCH comprised of a temporal series of spectra taken at the same pointing but at successive times. The images

Send offprint requests to: J.G Doyle

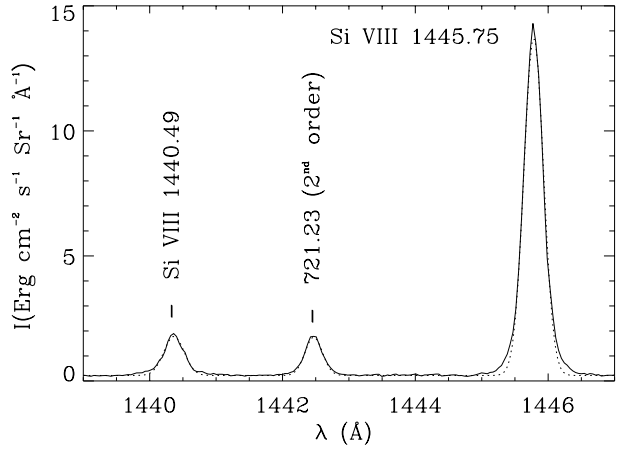

Fig. 1. A sample plot of the Si VIII spectral region in the coronal hole. Line fits are given by the dotted line.

were taken with the 1×300 and 4×300 arc sec slits. Using the individual spectra a summed spectrum was obtained. Analysis at different positions along the slit will give us information at different heights above the coronal hole. Details on the reduction procedures can be found in BTDW, where they have studied up to 1.25 $R_\odot$ off the limb. In the present paper we extend the analysis further off the limb up to 1.38 $R_\odot$.

For each line a Gaussian fit (Fig. 1) was applied using the Genetic Algorithm (GA) of Charbonneau (1995). A single Gaussian fit was applied for the analysis of each line. A complete examination of the reliability of GA with respect to other algorithms was performed by McIntosh et al. (1998). An estimation of the errors in the derived parameters was obtained using the GA-derived parameters as an input for a "classical" IDL-CURVEFIT procedure (Peter, 1999; Peter & Judge, 1999).

Using the new algorithms we re-analyze the dataset already presented by BTDW. For the NPCH, we add 3 more points at 285, 325 and 370 arcsec above the solar limb with respect to the data presented in BTDW. We find that our previous estimate of errors around 0.5 km s^{-1} for the non-thermal velocity obtained with the 1×300 slit and of 1.0–1.5 km s^{-1} for those obtained with the 4×300 slit, are correct. Slightly larger errors are present towards the end of each slit (see Sect. 3 and Fig. 4. later). For the new 3 points, errors of 4, 5 & 7 km s^{-1} were derived. For the electron density, the error arises not only from the measured ratio of the two lines but also from the errors in the atomic CHIANTI (Dere et al. 1997) database that we have used. The expected error coming from the database is estimated to be from 12% to 15% (see Laming et al., 1997). The propagation of this error in the ratio through the CHIANTI database was simply performed introducing the value of the ratio and the value of the ratio plus/minus the error. The resulting relative error was summed quadratically with the error of 15% estimated before. The final error was practically dominated by the errors in the database up to 200 arcsec (substantially the entire dataset presented in BTDW). Larger errors are again present for the new 3 points (see Fig. 2, inset).

Inspection of the spectral region around the Si VIII lines revealed a strong feature at 1442.47 Å, (identified as a second order line at 721.23 Å from a comparison of off-limb data taken on and off the KBr coated part of the detector; Feldman et al. 1997). The intensity variation of this line compared to Si VIII 1445.75 Å and 1440.49 Å shows a similar fall-off implying a similar temperature of formation. No identification was given by Feldman et al. (1997) of this line, although they did suggest it to be a hot coronal feature, perhaps due to Fe VIII. We are unable to verify its identification due to incomplete energy levels for Fe VIII.

3. Results and discussion

In Fig. 2, we plot the electron density as derived from Si VIII, coupled with N_e from UVCS (Kohl et al. 1998) and LASCO (Lamy et al. 1997). The LASCO data was acquired in February 1996, while the UVCS images were time-averaged from November 1996 to April 1997.

Guhathakurta & Fisher (1995, 1998) estimated the electron density distribution in the coronal hole from observations made with the space based SPARTAN 201–01,03 instrument. At that phase of the descending solar magnetic activity cycle the coronal conditions were different from our observing period (during our observing period the solar activity was in the minimum phase), so we don't compare our results with SPARTAN, but the essential density profile has a striking similarity. The above authors obtained the density profile from polarized brightness (pB) measurements between 1.16–6 $R_\odot$. They give an analytic prescription of the density profile as,

$$\frac{N(r)}{N(R_\odot)} = \exp\left[-\frac{\mu m_p g_\odot R_\odot}{k_B(T_e+T_p)/2}\left(1-\frac{R_\odot}{r}\right)\right] \quad (1)$$

where N is the number density (= $N_e + N_p$), μ is mean atomic weight (= 0.62), m_p the proton mass, k_B the Boltzmann constant, $g_\odot$ the solar gravity and the effective temperature is given by $T_{eff} = (T_e + T_p)/2$, where T_e and T_p are the electron and proton temperature, respectively. The line fit as a function of $(1 - \frac{R_\odot}{r})$ for all densities out to 8 $R_\odot$ is shown as the solid line in Fig. 2 for T_{eff} = 1.2 10^6 K. Thus for a locally isothermal fully ionized two-fluid coronal plasma solution we can either estimate T_e or T_p. Using T_e of Si VIII as 8 10^5 K (i.e. its formation temperature in ionization equilibrium), we find an estimate of T_p as 1.6 10^6 K. Furthermore this formula predicts an electron density of 4.5 10^3 cm^{-3} at 8 $R_\odot$ in excellent agreement with observations.

Our results for the ion temperature are in agreement with observations obtained by UVCS (Kohl et al. 1997; Cranmer et al. 1999) who find that at larger distances from the limb the ions in a coronal hole are extremely 'hot' and the electrons are much 'cooler'. Thus our observations re-confirms that in the coronal hole plasma, particularly at larger distances from the limb the assumption of collisional ionization equilibrium can not be used any more. This is also consistent with a study of several ions by Tu et al. (1998) who found ion temperatures perhaps as high as

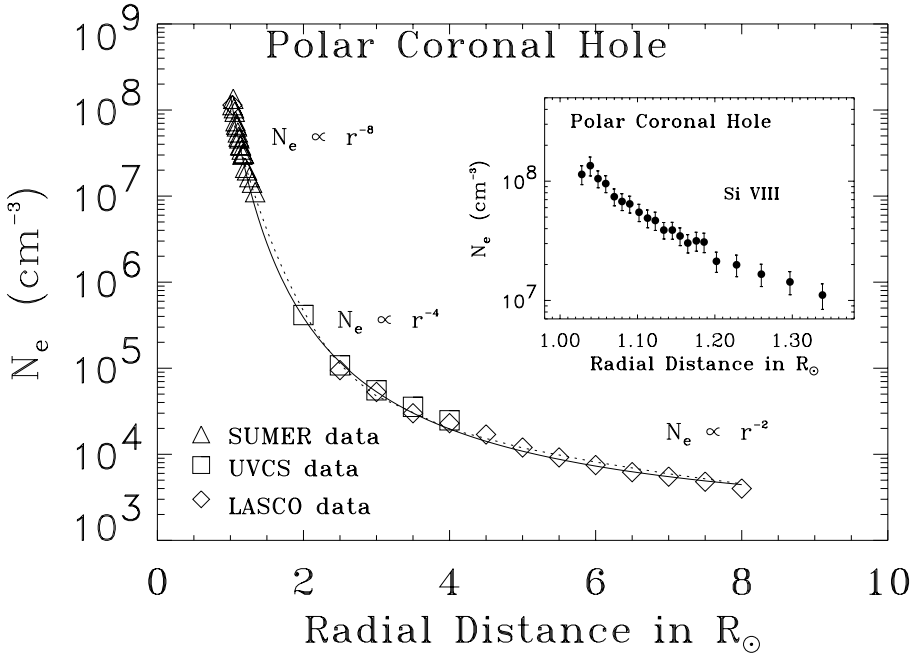

Fig. 2. Variation of the electron density above the polar coronal hole. The circles represent data from SUMER, diamonds data from LASCO and triangles data from UVCS. The solid line represents Eq. (1) with T_{eff} = 1.2 10^6 K and the dashed line represents the polynomial Eq. (2).

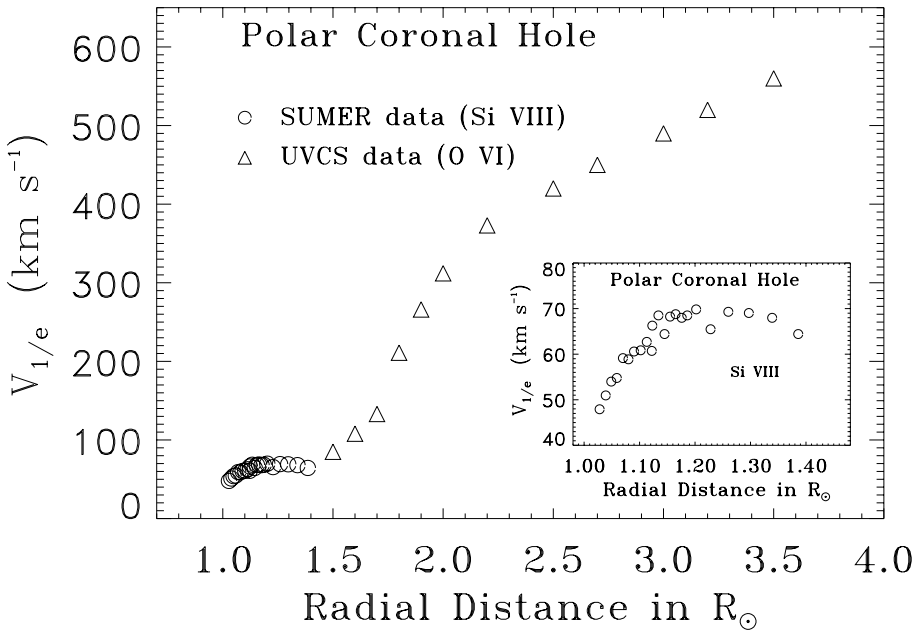

Fig. 3. Variation of the half width in km s^{-1} at $1/e$ of the peak intensity in the coronal hole. The circles represent data from SUMER and triangles data from UVCS.

2–3 times the formation temperature in ionization equilibrium even at heights of only a few tens of arcsecs.

Recently, Esser et al. (1999) have combined data from SPARTAN, White light coronagraph (WLC) from 1.5–5.5 $R_\odot$ in April '93, with Mauna Loa observations between 1.16–1.5 $R_\odot$ (Fisher & Guhathakurta, 1995). We are unable to fit the data in Fig. 2 with their polynomial as our data-set is more complete, extending from 1.02–8 $R_\odot$. In-fact, the expression given by Esser et al. predicts a rather high electron density at the limb and a density three orders of magnitude smaller at 1AU. Instead, the data in Fig. 2 suggests a fall-off in density proportional to r^{-8} from 1 to 2 $R_\odot$, then r^{-4} from 2 to 4 $R_\odot$ and finally as r^{-2}. A polynomial fit of the form

$$N_e = \frac{1 \times 10^8}{r^8} + \frac{2.5 \times 10^3}{r^4} + \frac{2.9 \times 10^5}{r^2} \qquad (2)$$

provides an excellent fit to the data as shown by the dotted line in Fig. 2. The first coefficient in the R.H.S of Eq. (2) is determined by the electron density close to the limb (i.e. from our Si VIII SUMER data), the last coefficient determined by the electron density at 1 AU, while only the middle coefficient was varied in order to provide the best fit.

In Fig. 3, we plot the half width at 1/e of the peak intensity ($V_{1/e}$) in km s^{-1} as measured from Si VIII SUMER data plus O VI UVCS data (Kohl et al. 1998). The effective (ion kinetic) temperature (T_k) can be obtained from (Kohl et al. 1998),

$$V_{1/e} = \frac{c\Delta\lambda_{1/e}}{\lambda_0} = \sqrt{\frac{2k_BT_k}{M}} \quad (3)$$

where M is the ion mass and $\Delta\lambda_{1/e}$ is the observed 1/e half width. We have applied a mass correction factor of 1.32 to the Si VIII data to make it consistent with O VI. Note that the kinetic temperature include contributions both from microscopic thermal motions and unresolved transverse wave motions. As shown in Fig. 3, this data suggests a small increase from 1 to 1.2 $R_\odot$, then a plateau up to 1.5 $R_\odot$, followed by a sharp increase up to 2 $R_\odot$, then a more gradual increase further out.

Now we turn our attention to the question of the non-thermal velocity. The analysis of DBP and BTDW showed that the non-thermal line-of-sight velocity as derived from the Si VIII line widths increases above the limb while the electron density decreases. On a closer inspection, the observations revealed that the non-thermal velocities were inversely proportional to the quadratic root of the electron density, in excellent agreement with that predicted for undamped radially propagating Alfvén waves. In the WKB approximation the rms wave velocity amplitude and density are related by (Hollweg 1990),

$$\left\langle \delta v^2 \right\rangle^{1/2} \propto \rho^{-1/4} \quad (4)$$

The non-thermal velocity can be deduced from the standard equation for an optically thin line broadened by thermal broadening caused by the ion temperature T_i and broadening caused by non-thermal motions as given by,

$$FWHM = \left[4ln2 \left(\frac{\lambda}{c}\right)^2 \left(\frac{2k_BT_i}{M} + \xi^2\right)\right]^{1/2} \quad (5)$$

where M is the ion mass, ξ is the non-thermal speed, related to the wave amplitude by $\xi^2 = \frac{1}{2}\left\langle \delta v^2 \right\rangle$, where the factor of 2 accounts for the polarization and direction of propagation of a wave relative to the line of sight.

Measuring the $FWHM$ of the Si VIII 1445 line and using Eq. (5) with $T_i \sim 1.6\ 10^6$ K (as suggested from the line fitting to N_e), the diamond symbols in Fig. 4 represents the observed non-thermal velocities at different heights.

Now If we assume the same ion temperature as Si VIII for the 721.23 Å line (as suggested by the intensity fall-off compared to Si VIII), the Si VIII non-thermal widths implies an ion mass of ∼53 for this new feature. This latter assumption is probably valid as different emission lines are generated in the same column mass as seen by the spectrograph. Although, this can not be taken as absolute proof it does suggest that the line may be due to Fe, probably ionization stages VII–VIII.

In Fig. 4, the (+) represents the velocities calculated on the basis of the Eq. (4), using the measured N_e from Si VIII. We have used a magnetic field strength of $B = 6G$ and a proportionality constant so as to match the energy flux density (see BTDW for details). In both cases, we find excellent agreement in the inner corona, but for the outer corona $\gg$ 200 arc sec (see Fig. 4), the (+) symbols starts to deviate from those calculated from the observed $FWHM$(diamond symbols in Fig. 4). It is also possible to estimate the errors in the calculated non-thermal velocity (+); for the last 4 points, errors of 3, 3, 5 and 15 km s^{-1} have been estimated. Despite these large errors we have no overlap with the error-bars of the observed non-thermal velocities, suggesting an effective break-down of Eq. (4) above 1.2 $R_\odot$.

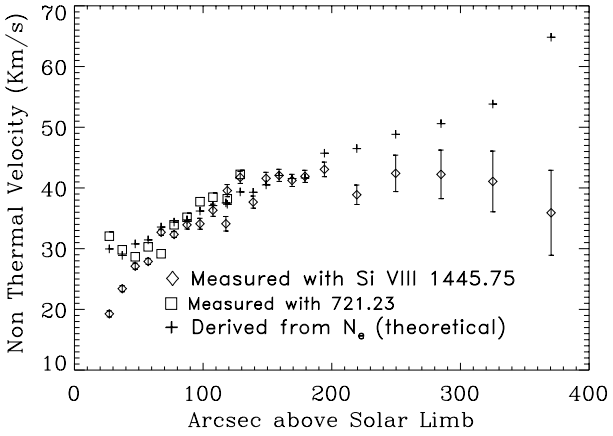

Fig. 4. Variation of the non-thermal velocity with height in the north polar coronal hole. The diamonds represent those measured with Si VIII, the plus symbols correspond to theoretical estimates based on Eq. (4) and the measured N_e (see text) and squared boxes represent those derived from the 721.23 Å line assuming it's due to an Fe ion.

Lou & Rosner (1994) have already pointed out that waves can be reflected against gradients in the Alfvén speed and the WKB approximation fails. The reflection is important as it increases the momentum transfered from the Alfvén wave to the medium. Recently Torkelsson et al. (1998) have shown that the Alfvén waves steepen and produce current sheets in the non-linear regime. These waves are strongly damped by non-linear steepening. They have also reported density oscillations in their simulations, which are consistent with observations by Ofman et al. (1997) who reported quasi periodic variations in the polarized brightness in the polar coronal holes between 1.9–2.45 $R_\odot$, as observed from the white light channel (WLC) of UVCS. It would be interesting to see whether these density oscillations are also present in the inner corona which can be due to the presence of non-linear high amplitude compressional waves as reported by Ofman et al. (1997). For that one needs a high cadence dataset. We propose that somewhere around 1.2–1.3 $R_\odot$ this non-linearity becomes important (as indicated by Figs. 3 & 4). The Alfvén waves with an amplitude of 30–50 km s^{-1} (as observed) at the base of the coronal hole can generate non-linear solitary type of waves, which can contribute significantly to solar wind acceleration in open magnetic field structures.

Note from Fig. 3 that relatively sharp variations occur around 1.5 $R_\odot$. This may be the location where the thermalization and the isotropization times of various species begins to exceed the local coronal expansion time. Esser et al. (1999) from a study of Mg X and O VI lines (observed with *SOHO*/UVCS) found a transition from collisional to collisionless plasma between 1.75 to 2.1 $R_\odot$ in a polar coronal hole. Cranmer et al. (1999) have presented an empirical model of H I and O VI distributions, which also indicates the presence of this transition. In their model they found a sharp variation between 1.8 $R_\odot$ -

2.1 $R_\odot$ (see their Figs. 5&9). It is also interesting to note that the electron density variation at 2 $R_\odot$ has changed to r^{-4} from its earlier r^{-8} fall-off. For line width measurements, UVCS data are not available below 1.5 $R_\odot$, so we feel that the combined SUMER and UVCS datasets allows us to locate this transition point with better precision suggesting that the physics of the plasma transport and wave dissipation diverges from classical Coulomb theory at heights beyond 1.5 $R_\odot$. At larger distances, e.g. above 2 $R_\odot$, the large $V_{1/e}$ can also be due in part to the ion-cyclotron resonant acceleration by high frequency MHD waves (McKenzie et al. 1995). We hope that our results will provide more precise input parameters at the base of the coronal hole for future solar wind models.

Acknowledgements. Research at Armagh Observatory is grant-aided by the Department of Education for N. Ireland while partial support for software and hardware is provided by the STARLINK Project which is funded by the UK PPARC. This work was supported by PPARC grant GR/K43315. We would like to thank the SUMER team at Goddard Space Flight Center for their help in obtaining the data. The SUMER project is financially supported by DLR, CNES, NASA, and PRODEX. SUMER is part of *SOHO*, the Solar and Heliospheric Observatory of ESA and NASA. We would also like to thank Scott McIntosh for a copy of the GA routine.

References

Arnaud M., Rothenflug R., 1985, A&AS 60, 425
Banerjee D, Teriaca L., Doyle J.G., Wilhelm K., 1998, A&A 339, 208
Brueckner G.E., Howard R.A., Koomen M.J., et al., 1995, Sol. Phys 162, 357
Charbonneau P., 1995, ApJS 101, 309
Cranmer S.R., Kohl J.L., Noci G., et al., 1999, ApJ 511 481
Dere K.P., Landi E., Mason H.E., Monsignori fossi B.C., Young P.R., 1997, A&AS 125, 149
Doschek G.A., Warren H.P., Laming J.M., et al., 1997, ApJ 482, L109
Doyle J.G., Banerjee D., Perez M.E., 1998, Sol. Phys 181, 91
Doyle J.G., Keenan F.P., Ryans R.S.I., Aggarwal K.M., Fludra A., 1999, A&A (submitted)
Esser R., Fineschi S., Dobrzycka D., et al., 1999, ApJ 510, L63
Feldman U., Behring W.E., Curdt W., et al., 1997, ApJS 113, 195
Fisher R., Guhathakurta M., 1995, ApJ 447, L139
Fludra A., Del Zanna G., Bromage B., 1999a, Space Sci. Rev, (submitted)
Fludra A., Del Zanna G., Alexander D., Bromage B.J.I., 1999b, J. Geophys. Res., (in press)
Guhathakurta M., Fisher R., 1998, ApJ 499, L215
Guhathakurta M., Fisher R., 1995, GRL 22(14), 1851
Harrison R.A., et al., 1995, Sol. Phys. 162, 233
Hassler D.M., Rottman G.J., Shoub E.C. Holzer T.E., 1990, ApJ 348, L77
Hollweg J.V., 1990, Computer Phys. Reports 12, 205
Kohl J.L., Noci G., Antonucci E., et al., 1995, Sol. Phys 162, 313
Kohl J.L., Noci G., Antonucci E., et al., 1997, Sol. Phys 175, 613
Kohl J.L., Noci G., Antonucci E., et al., 1998, ApJ 501, L127
Laming J.M., Feldman U., Schühle U., et al., 1997, ApJ 485, 911
Lamy P., Quemerais E., Liebaria A., et al., 1997, Fifth SOHO Workshop, ESA SP-404, p. 491
Lou Y.Q., Rosner R., 1994, ApJ 424, 429
McKenzie J.F., Banaszkiewicz M., Axford W.I., 1995, A&A 303, L45
McIntosh S.W., Diver D.A., Judge P.G., et al., 1998, A&AS 132, 145
Ofman L., Romali M., Poletto G., Noci G., Kohl J.L., 1997, ApJ 491, L111
Peter H., 1999, ApJ 516 (in press)
Peter H., Judge P.G., 1999, ApJ (submitted)
Torkelsson U., Boynton G.C., 1998, MNRAS 295, 55
Tu C.-Y, March E., Wilhelm K., Curdt W., 1998, ApJ 503, 475
Warren H.P., Hassler D.M., 1999 (pre-print)
Wilhelm K., Curdt W., Marsch E., et al., 1995, Sol. Phys 162, 189
Wilhelm K., Marsch E., Dwivedi B.N., et al., 1998, ApJ 500, 1023